Nitrobenzene "Caged" Compounds as Irreversible Photoreductants: A Rational Approach to Studying Photoinduced Intermolecular Electron-Transfer Reactions in Proteins†

Theodore J. DiMagno, Michael H. B. Stowell, and Sunney I. Chan*

Arthur Amos Noyes Laboratory of Chemical Physics, 127-72, California Institute of Technology, Pasadena, California 91125

Received: June 8, 1995®

Nitrobenzene "caged" compounds are well-known for their use in delivering biologically active substrates to a reaction mixture after photoexcitation. We have discovered that they also behave as photoreductants from the triplet state after photoexcitation. To explore the properties of these newly discovered photoreductants, a series of substituted nitrobenzene derivatives have been synthesized. These nitrobenzene derivatives exhibit many desirable characteristics suitable for the physiological photoreduction of different proteins, and examples are shown for the photoreduction of cytochrome *c* and other heme proteins. The observed rate constant for photoreduction of cytochrome *c*, k_{obs}, ranges from 300 to 36 000 s^{-1} for the various nitrobenzene derivatives. pH and ionic strength experiments are consistent with a bimolecular reaction wherein the photoreductant and the protein form an electrostatic complex prior to electron transfer. A kinetic model for this bimolecular reaction is described and simulations of the experimental data for the photoreductant 4,5-dimethoxy-2-nitrophenylacetic acid (DMNPAA) yield an inherent unimolecular electron-transfer rate constant (k_{et}) of 14 600 s^{-1} for the photoreduction of cytochrome *c* at pH 6.6.

Introduction

Over the past 10 years, photoactivatable "caged" probes have been used to control the spatial and temporal release of biologically active substrates in molecular biophysics. The caging group is designed to detach from the biological substrate after illumination with UV radiation (<360 nm) to generate a burst of substrate in the millisecond to microsecond time scale. This temporal release of substrate has allowed the kinetic measurements in a wide variety of applications such as the following: photoinitiated nucleotide release to study skinned muscle fibers,[1-3] erythrocyte ghosts,[4] sarcoplasmic reticulum vesicles,[5] skeletal muscle fibers,[6] and G-proteins;[7,8] photoinitiated calcium release[9] or calcium scavengers;[10] photoinitiated neurotransmitter release to initiate or block neurotransmitter action;[11-13] or photoinitiated amino acid release to study such processes as the functional circuitry in the brain.[14]

Recently, we have discovered that these photoactivatable "caged" probes are facile in their photoreduction of proteins as well. These derivatives function as photoreductants because of the large redox driving force of the nitrobenzene moiety when they are photoactivated into the triplet state (>2 V[15]). Because of the intramolecular rearrangement process that these nitrobenzene derivatives undergo upon photolysis (process which releases the substrate from the cage), these compounds behave as irreversible electron-transfer donors. In addition, these photoreductants can be synthetically modified to rationally design the absorption profile of these electron donors to minimize the overlapping absorption transitions with the protein of interest. The synthetic manipulation of the nitrobenzene derivatives also allows control of the charged groups on the photoreductant to optimize maximum binding between the donor and protein; in this manner, the observed electron transfer rate can be controlled and maximized.

A number of different methods have been developed for the rapid reduction of proteins necessary for studying electron-transfer events. Pulse radiolysis was one of the first techniques used for determining the kinetic behavior of one electron reductions of a variety of different proteins.[16-20] This technique uses the hydrated electron (e_{aq}^-) or weaker reductants such as the CO_2^- or 1-methylnicotinamide[21] radical to reduce the redox center. Another popular method is to use a reductant which donates an electron through a bimolecular process after being photoexcited by a laser. Several photoreductants have been used with success so far. These include porphyrins,[22,23] flavins,[24,25] ruthenium complexes,[26,27] and NADH.[28] A related method exploits ruthenium-labeled proteins[29,30] which can be photoexcited to initiate intramolecular first-order electron transfer to an electron acceptor within the protein.

Although all of the above photoexcitation methods have been successful, they all have certain disadvantages for studying enzymatic reactions. One major disadvantage is that the electron-transfer back reaction rate is on the same order as the forward electron transfer rate to the protein. Consequently, the net yield of photoreduced protein is often negligible. This has been overcome, for the most part, by adding sacrificial quenchers to rapidly rereduce the photoreductant in order to prevent the back-electron-transfer reaction from occurring. However, this solution creates added complications by having a radical quencher species as well as newly created radicals present in solution. In some cases, the radical species that are formed and the manner in which they react with the protein are unclear or unknown. Oftentimes, a more serious problem is that the photoreductants and quenchers used in the photoreduction process have absorption and emission bands from both the ground and excited states throughout the visible absorption region. This introduces a spectroscopic complexity that makes it necessary to deconvolute the observed transient signals from the real electron-transfer process of interest. The large signals from the electron donor and quencher in combination with the usually poor yield of the directly reduced protein can make deconvolution difficult. This particular situation is what prompted us to investigate the nitrobenzene photoreductants described in this study.

In this paper, we describe the properties of a series of substituted nitrobenzene derivatives (Figure 1) designed to act as photoreductants. As an example of the utility of these new

† Contribution No. 9014 from the Division of Chemistry and Chemical Engineering, California Institute of Technology.

* To whom correspondence should be addressed.

® Abstract published in *Advance ACS Abstracts*, August 1, 1995.

0022-3654/95/2099-13038$09.00/0

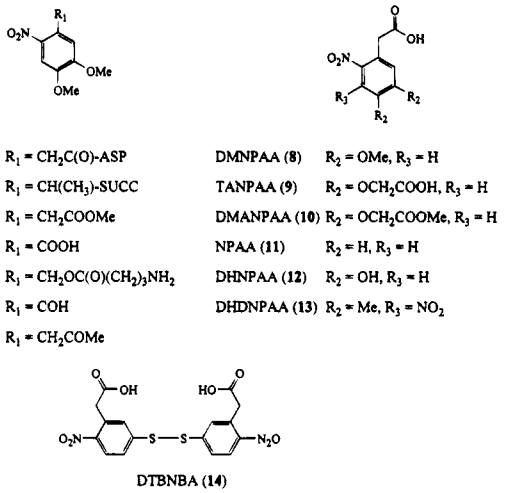

Figure 1. Structures of the 14 different nitrobenzene derivatives tested for their ability to photoreduce cytochrome *c*. Table 1 lists the observed electron transfer rate constants for the photoreduction of cytochrome *c*.

SCHEME 1

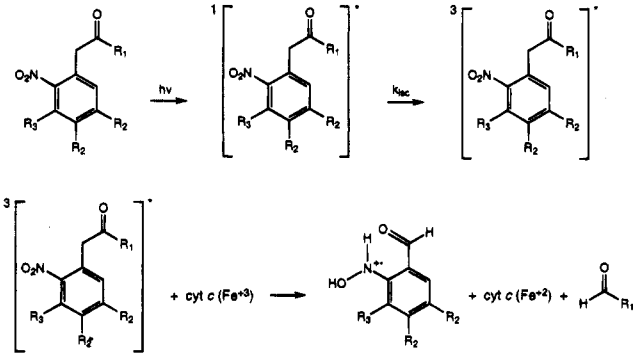

nitrobenzene derivatives, the photoreduction of cytochrome *c* and other heme proteins (indicated in Scheme 1) was investigated. We feel that this series of nitrobenzene derivatives exhibits many of the desired characteristics for a suitable photoreductant for protein systems. First, the photoreductant undergoes internal quenching via irreversible photochemistry following electron transfer to the protein so that no back electron transfer is observed. Second, the absorption profile of the photoreductant and photoproducts has no absorption or emission bands with wavelengths >430 nm that will overlap and interfere with the prosthetic groups of the protein. In addition, the absorption profile can be partially tuned by synthetically modifying the various substituents on the parent nitrobenzene (R1, R2, and R3 in Scheme 1) to avoid spectral overlaps among the various species in solution. Third, the nitrobenzene derivatives do not reduce other species in the solutions used for these experiments. Fourth, because of the large yield of reduced protein and the excellent signal-to-noise ratio, the nitrobenzene photoreductants allow enzymatic processes to be studies in the single turnover mode, thus allowing the physiological process to be studied. In the single-turnover mode, photoreductants that rely on multiple-shot signal averaging to obtain a high signal-to-noise ratio cannot be used because a distribution of enzyme intermediates become populated and a heterogeneous mixture results.

To illustrate, we report here the effects of pH, ionic strength, and the various substituents on the rate of electron transfer from the nitrobenzene photoreductants to cytochrome *c*. In a future paper, we will describe the use of these nitrobenzene photoreductants to examine the intermolecular electron transfer between cytochrome *c* and its physiological electron-acceptor cytochrome *c* oxidase under various conditions of activation of the oxidase.

TABLE 1: Single-Exponential Fit for the Photoreduction of Cytochrome c by the Nitrobenzene Photoreductants[a]

photoreductant	R1	R2	R3	k_{obs} (s^{-1})
DMNPA-ASP	$CH_2C(O)$-Asp	OMe	H	12100
SUCC	$CH(CH_3)$-Succ	OMe	H	10300
DMNPAA	CH_2COOH	OMe	H	8900
DANPATA	CH_2COOH	OCH_2COOH	H	7200
MDMNPA	CH_2COOMe	OMe	H	6300
DMANPAA	CH_2COOH	OCH_2COOMe	H	5900
DMNBA	COOH	OMe	H	5500
DTBNBA[b]	COOH	S-	H	5300
GABA	$CH_2OC(O)(CH_2)_3NH_2$	OMe	H	5300
DMNB	COH	OMe	H	5200
DMNAP	CH_2COMe	OMe	H	3300
NPAA	CH_2COOH	H	H	300
DHNPAA	CH_2COOH	OH	H	
DHDNPAA	CH_2COOH	OH	NO_2	

[a] Substituents R1, R2, and R3 as positioned in Figure 1. Experimental conditions were 100 mM ADA buffer, pH 6.6, 15 μM cyt c, and 100 μM photoreductant. Photoexcitation was initiated with a Nd:YAG laser fired at a repetition rate of 1 Hz with 1.5 mJ/pulse. [b] Dimer linked through disulfide bond between two monomers at R2 position as shown in Figure 1.

TABLE 2: Electron-Transfer Rates from DMNPAA to Several Heme Proteins[a]

protein	k_{obs} (s^{-1})	pI
cytochrome *c*	8900	10.4
hemoglobin	730	7.7
myoglobin	390	6.8
peroxidase	91	7.2

[a] Experimental conditions the same as described in Table 1 except that hemoglobin, myoglobin, and peroxidase were all at 20 μM. The fits listed in Table 2 were obtained by fitting the data to a single exponential. However, a biexponential fit gave much better results for hemoglobin, myoglobin, and peroxidase (see Figure 8 for biexponential fits).

In general, the binding properties of these nitrobenzene electron donors with any protein acceptor may be altered by appropriate substituents on the parent nitrobenzene framework, thus maximizing the intermolecular electron transfer to the physiological electron donor in these protein complexes. For the cytochrome *c*/cytochrome *c* oxidase complex, K_M and V_{max} are unaffected by the presence of these nitrobenzene photoreductants.

Results

Table 1 shows the results for the single exponential fit, k_{obs}, for the photoreduction of cytochrome *c* via the 14 different nitrobenzene derivatives in order of decreasing rates. Figure 2 shows a typical kinetic trace for the photoreduction of cytochrome *c* by DMNPAA at 550 nm. The fastest electron transfer to cytochrome *c* in 100 mM *N*-2-acetamidoiminodiacetic acid (ADA) buffer was k_{obs} = 12 100 s^{-1} ($\tau \approx 90$ μs) for the DMNPA-ASP derivative, and the slowest electron input was k_{obs} = 300 s^{-1} for the NPAA derivative under identical experimental conditions. The two dihydroxy derivatives (DHNPAA and DHDNPAA) showed no electron transfer to cytochrome *c*. However, this is most likely caused by either the lack of photoexcitation of these two derivatives due to the small cross-sectional area at 355 nm (the absorption maxima have shifted to ≈420 nm in these photoreductants) or the possible altered photophysics that these dihydroxy derivatives may exhibit.

The amount of cytochrome *c* reduced by the nitrobenzene photoreductant per laser flash is dependent on the photoreductant concentration and laser power. The yield of reduced cytochrome *c* increases with increasing donor concentration and there is a linear dependence of the yield on the *observed* reduction rate (Figure 3). In order to extract the rate constant for the electron transfer to cytochrome *c* for the second order bimolecular process, a study of rate versus cytochrome *c* concentration was

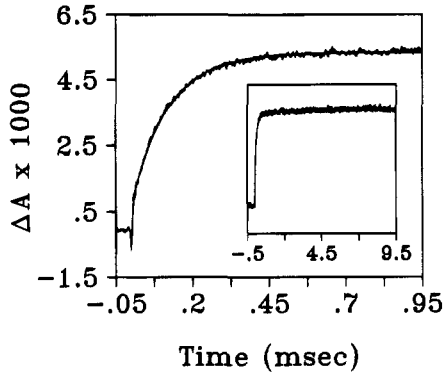

Figure 2. Typical transient absorption kinetics for the reduction of cytochrome *c* at 550 nm from the photoreductant DMNPAA. The experimental conditions were 15 μM cytochrome *c* and 100 μM DMNPAA in 100 mM ADA buffer, pH 6.6. DMNPAA was excited at 1 Hz with a Nd:YAG laser at 355 nm (1.5 mJ/pulse at the sample), and approximately 0.3 μM of cytochrome *c* was reduced per laser flash (2%). The kinetic curve is the average of two laser shots, and the single-exponential fit gave $k_{obs} = 8900\ s^{-1}$. The inset shows the cytochrome *c* kinetics at 550 nm over a longer time scale to show that no back electron transfer to the nitrobenzene photoreductant occurs.

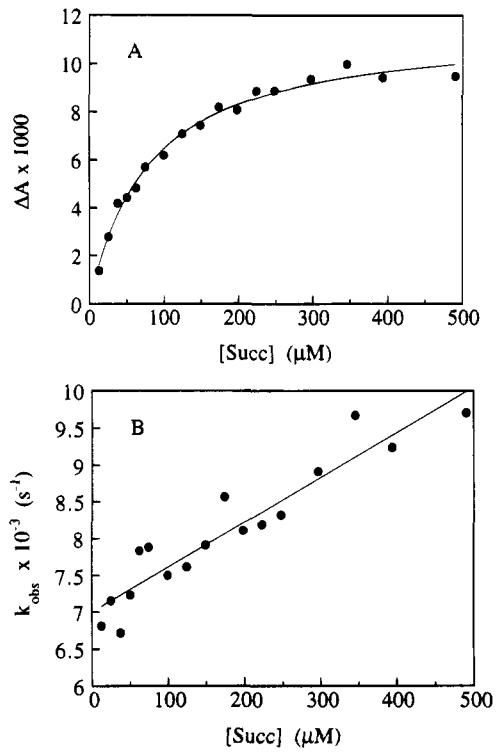

Figure 3. (A) Yield of reduced cytochrome *c* increases with a hyperbolic dependence (solid line) as the concentration of the photoreductant SUCC increases. Each point is the average of five laser shots, and ΔA was determined from the constant obtained with a single-exponential fit of the transient kinetic data. The experimental conditions were the same as given in Figure 2 except that the SUCC was used instead of DMNPAA as the photoreductant. (B) Single-exponential fit (k_{obs}) for the formation of reduced cytochrome *c* at 550 nm increases linearly (solid line) as the concentration of the photoreductant SUCC increases. The exponential fit was obtained from the same data that was used in (A).

performed (Figure 4). Over the range of concentrations of cytochrome *c* that were used in the transient absorption measurements, the rates increase linearly and did not saturate as would be expected for typical bimolecular kinetics. Therefore, only approximate limits could be placed on the electron-transfer rate constant using this analysis (see discussion for a complete analysis of the electron-transfer rate constant, k_{et}).

Laser Power Dependence. The observed electron-transfer rate to cytochrome *c* and the yield of reduced cytochrome *c*

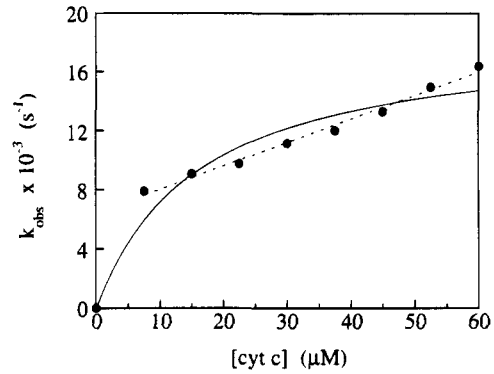

Figure 4. Electron transfer from the photoreductant DMNPAA to cytochrome *c* measured as a function of cytochrome *c* concentration from 7.5 to 60 μM. The data were fit to both a hyperbolic dependence (solid line) and a linear dependence (dashed line). Since the linear fit was much better than the expected hyperbolic dependence for the bimolecular process, the electron-transfer rate constant could not be reliable determined from these data. The experimental conditions were the same as given in Figure 2.

were measured as a function of the laser power (0.2−4.0 mJ/pulse). The observed electron-transfer rate remained constant over all pulse energies used, and the yield of reduced cytochrome *c* increased linearly with increasing laser power (data not shown). These results indicate that the electron transfer is a one-photon, single-electron-transfer event. Further evidence for a single-electron-transfer event was obtained by photoexciting a 1:3 mixture of DMNPAA:cytochrome *c* and obtaining only 1 equiv of reduced cytochrome *c* after exhaustive excitation at 355 nm (data not shown).

pH and Ionic Strength Dependence on Electron Transfer. The dependence of the electron transfer as a function of pH was probed with DMNPAA as the photoreductant. Two trends were observed for this reaction. First, the yield of reduced cytochrome *c* increased as the pH increased. Figure 5A shows the steady-state reduced minus oxidized difference spectra of the sample after 50 laser shots, and Figure 5B shows the transient spectrum obtained from the same sample, while Figure 6A shows the change in absorption at two wavelengths from the reduced minus oxidized difference spectra in Figure 5A. Second, the observed rate of electron transfer to cytochrome *c* decreased as the pH increased (Figure 6B).

The two trends observed for the ionic strength dependence were similar to those observed for the pH dependence. The ionic strength was changed by varying either the ADA buffer concentration as shown in Figure 7A or the NaCl concentration as shown in Figure 7B. The variation in the ADA buffer concentration for the triacid photoreductant DANPATA showed an increase in the yield of reduced cytochrome *c* (both transient and steady-state yields) and a decrease in the observed electron-transfer rate as the ionic strength was increased. When the ionic strength was increased with NaCl, the observed rate of electron transfer also decreased, but to a much smaller extent than the ADA ionic strength dependence. This smaller decrease was due to the higher initial ionic strength in the NaCl dependence from the ADA buffer itself (50 mM). When comparing the NaCl dependence starting at 50 mM with the ADA dependence, then the magnitude of the rate decrease is roughly the same for both methods of changing the ionic strength (Figure 7A). However, when the ionic strength was increased with NaCl, the yield of reduced cytochrome *c* decreased, in contrast to the ADA dependence. A decrease in yield is expected as the ionic strength is increased because the binding affinity of the photoreductant DANPATA to cytochrome *c* decreases with increasing ionic strength. The results from the ADA ionic strength dependence seem anomalous in this light, but the

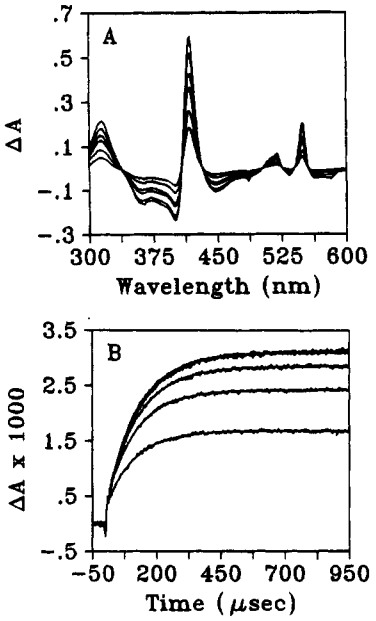

Figure 5. (A) Reduced minus oxidized difference spectra for cytochrome *c* as a function of pH obtained by photoreduction with DMNPAA after 50 laser shots. The yield of reduced cytochrome *c* increase as the pH increased from pH 6.0 (smallest signal at 550 and 418 nm), pH 6.4, pH 6.8, pH 7.2, pH 7.6, to pH 8.0 (largest signal at 550 and 418 nm). (B) Transient kinetics for the reduction of cytochrome *c* at 550 nm as a function of pH. The range of pH values was the same as given in (A). The smallest transient signal in (B) was at pH 6.0, and the signal increased with increasing pH. The transient signals for pH 7.2, pH 7.6, and pH 8.0 all have essentially the same magnitude, but their k_{obs} obtained from a single-exponential fit decrease slightly. k_{obs} = 9100 s^{-1} (pH 6.0), k_{obs} = 8800 s^{-1} (pH 6.4), k_{obs} = 8100 s^{-1} (pH 6.8), k_{obs} = 8000 s^{-1} (pH 7.2), k_{obs} = 7600 s^{-1} (pH 7.6), and k_{obs} = 7700 s^{-1} (pH 8.0). The experimental conditions were the same as given in Figure 2.

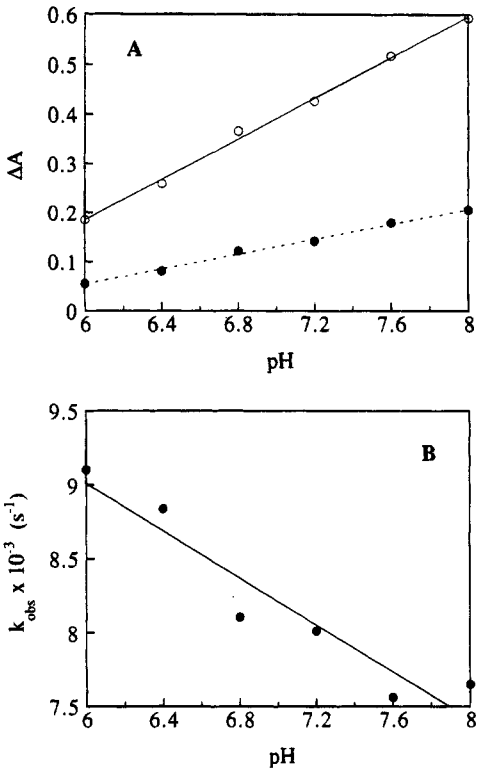

Figure 6. (A) Yield of reduced cytochrome *c* increases linearly as a function of increasing pH at both 418 nm (○) and 550 nm (●). The data points are extracted from the steady-state reduced minus oxidized difference spectra for cytochrome *c* shown in Figure 5A. (B) Observed rate of reduction of cytochrome *c* as a function of pH. The data are the single-exponential fits to the transient decay curves shown in Figure 5B.

observations here are most likely related to the enhanced electron-transfer yield observed for ADA over other buffers such as phosphate, TRIS·HCl, and HEPES and do not represent an ionic strength dependence. This enhanced reduced cytochrome *c* yield is thought to be from the ability of ADA to complex free metals in solution which quench the excited state of the photoreductant.[31] In support of this hypothesis, the photoreduction of cytochrome *c* by DMNPAA was effectively quenched by the addition of metal ions (Cu^+, Fe^{2+}, Zn^{2+}) into the reaction mixture (data not shown). This would explain the observed increase in the reduced cytochrome *c* yield as the ADA concentration is increased and the variable yield of reduced cytochrome *c* observed in HEPES buffer.

Electron Transfer to Other Heme Proteins. DMNPAA is also an effective electron donor for other proteins. Myoglobin, hemoglobin, and peroxidase were all photoreduced by DMNPAA under both aerobic and anaerobic conditions. Under aerobic conditions, the observed electron-transfer rate constant was often difficult to extract because the reoxidation by dioxygen was on the same time scale as the photoreduction and the errors in the deconvolution process became large. Under anaerobic conditions, however, no reoxidation was detected and the observed electron-transfer rate was measured to be k_{obs} = 390 s^{-1} for myoglobin (20 μM), k_{obs} = 730 s^{-1} for hemoglobin (20 μM), and k_{obs} = 91 s^{-1} for peroxidase (20 μM) under identical experimental conditions (Figure 8). The fast phase of the photoreduction observed for all three species (τ < 1 μs) is due to the direct photoexcitation of these heme proteins as previously observed by Gu et al.[32] and is observed in the absence of the DMNPAA photoreductant.

Discussion

Ideally a photoreductant should have several characteristics. First, the radical cation photoproduct produced must exhibit a slow or nonexisting back-electron-transfer reaction from the protein. This would increase the overall yield of reduction of the protein and make it unnecessary to add quenchers to the solution, which in turn would simplify the interpretation of the results. Second, the photoreductant and its final photoproduct should not have absorption or emission bands in the visible region which overlap with the protein prosthetic group being reduced and studied. Third, and a generally ignored property, the photoreductant should not reduce any other components of the system. Fourth, the photoreductant should not interfere with the binding of substrate(s) or other physiological processes involving the protein.

The nitrobenzene derivatives work well in their newly discovered use as photoreductants for several reasons. First, the photoreductant and its products are optically transparent throughout the visible region (λ > 430 nm) and thus do not interfere with the measurements of the heme chromophores. This precludes the need for deconvolution of complicated kinetics arising from several different species. Only the protein signal is observed in the visible region, and the data analysis is accordingly straightforward.

Second, no appreciable back electron transfer is observed over the time scale of the electron-transfer reactions to the protein. Figure 2 shows that the photoreduced cytochrome *c* does not decay over a 10 ms time scale in the presence of a 10-fold excess of DMNPAA (same results for the other donors). The back electron transfer does not occur because the photolytically oxidized DMNPAA is presumed to undergo an intramolecular rearrangement reaction to form the nitroxide species[33] (Scheme 1), which can disproportionate to form the stable ground-state

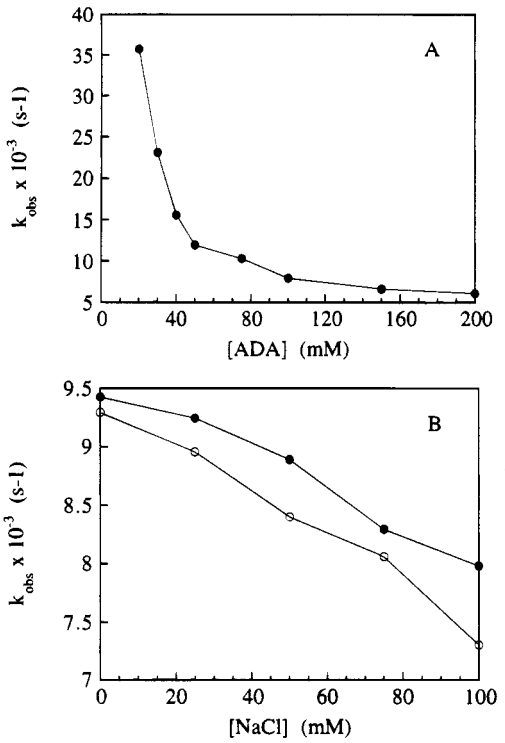

Figure 7. (A) Effect of the ionic strength ([ADA] dependence) on the electron transfer to cytochrome *c* from the photoreductant DANPATA. At [ADA] <20 mM, the transient signal-to-noise decreases too much to be reliably fit. Experimental conditions were 15 μM cytochrome *c*, 100 μM DANPATA, pH 6.6, and the [ADA] given for each point. (B) Effect of the ionic strength ([NaCl] dependence) on the electron transfer to cytochrome *c* from the photoreductant DANPATA at pH 6.4 (●) and 7.8 (○). The experiment conditions were 15 μM cytochrome *c*, 100 μM DANPATA, 50 mM ADA (to provide adequate signal-to-noise), and pH 6.4 (●) or pH 7.8 (○). The approximate linear dependence obtained in (B) is similar to the approximate linear region observed in (A) when the ADA concentration was above 50 mM.

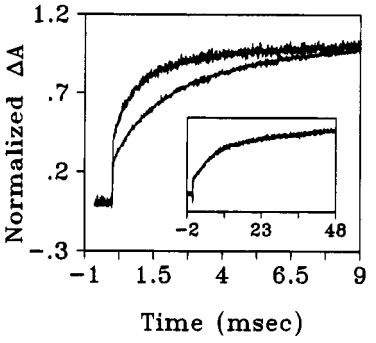

Figure 8. Transient absorption of the Soret band at 426 nm for the photoreduction of hemoglobin (upper kinetic trace), myoglobin (lower kinetic trace), and peroxidase (inset, expanded time scale) using DMNPAA as the photoreductant. The data shown here were fit to a biexponential decay (see Table 2 for a single-exponential fit). The two observed rate constants were $k^f_{obs} = 1500\ s^{-1}$ (62%) and $k^s_{obs} = 290\ s^{-1}$ (38%) for hemoglobin, $k^f_{obs} = 910\ s^{-1}$ (38%) and $k^s_{obs} = 210\ s^{-1}$ (62%) for myoglobin, and $k^f_{obs} = 160\ s^{-1}$ (27%) and $k^s_{obs} = 3.5\ s^{-1}$ (73%) for peroxidase, where k^f_{obs} and k^s_{obs} are the fast and slow components, respectively. The weighted average of the two exponentials approximates the single exponential value listed in Table 2. The experimental conditions were 20 μM protein (hemoglobin, myoglobin, or peroxidase), 100 μM DMNPAA, and 100 mM ADA at pH 6.6.

hydroxylamine- and nitrosobenzoic acid products. The nitroxide intermediate has been observed at 77 K by electron spin resonance (data not shown), the hydroxylamine photoproduct isolated, and its identity confirmed by GCMS. However, the rate of disproportionation of the nitroxide species has not been determined. Because these nitrobenzene photoreductants undergo this intramolecular rearrangement, no external quenchers are necessary to quench the radical cation donor species. This simplifies the experiment by reducing the number of chemical species in solution which can interact and interfere with electron transfer to the protein, an advantage that the other photoreducing systems do not have.

SCHEME 2

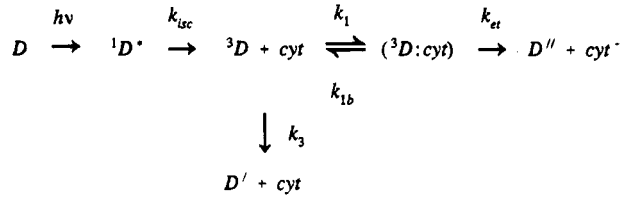

An important advantage of the nitrobenzene photoreductants is that they can be readily synthesized as well as modified with various substituents. This enables the absorption profile of the photoreductant to be shifted to either higher or lower energy to avoid overlapping absorption bands with the protein under study. Furthermore, the easy addition of charged substituents also makes it possible to engineer a specific photoreductant that can bind tightly to a desired protein of interest or even to be covalently bound to the amino acids of the protein with well-known coupling reactions. These derivatives could then be designed to function as unimolecular electron donors in the same manner that ruthenium-labeled cytochrome *c* derivatives have been used.[29,30] This flexibility may make these donors appropriate for many proteins other than the few examples examined in this introductory work.

Reaction Mechanism and Electron-Transfer Kinetics. Only the observed electron-transfer rate has been discussed for this bimolecular electron-transfer process. Even though k_{obs} for the photoreduction of cytochrome *c* is relatively slow ($\sim 10^4\ s^{-1}$) at the physiological ionic strength (100 mM) for the cytochrome *c*/cytochrome *c* oxidase redox partners, this does not mean that the inherent electron transfer between the nitrobenzene donor and cytochrome *c* is slow. Rather this indicates that the bimolecular process under the observed experimental conditions is slow. What is most important is the inherent electron-transfer rate, k_{et}, because this is the limit on how fast electron transfer can occur under optimal conditions.

A simplified reaction mechanism which includes all known chemical reactions for the photoreduction of cytochrome *c* is shown in Scheme 2, where D is the nitrobenzene donor; $^1D^*$ is the photoexcited singlet state of the donor; ^3D is the photoexcited triplet state of the donor, i.e., the species that initiates the electron-transfer chemistry; (^3D:cyt) is the bound complex; and D′ and D″ are the nitrobenzene product derivatives after the intramolecular photochemical rearrangement process or the intermolecular electron-transfer process, respectively. The kinetic pathway designated by k_3 describes the intramolecular photoinitiated rearrangement process that occurs in the absence of cytochrome *c* without electron transfer.[33] In the absence of this process, the reduction of cytochrome *c* can proceed no faster than the rate of formation of the complex ^3D:cyt.

The rate law for the kinetic mechanism described in Scheme 2 can be formulated in terms of the rate of formation of reduced cytochrome *c* (eq 1). The concentration of the bound DMNPAA:cytochrome *c* complex, [^3D:cyt], can be related to the concentration of its photoexcited precursor ^3D by the differential equation:

$$d[cyt^-]/dt = k_{et}[^3D{:}cyt] \quad (1)$$

$$d[^3D{:}cyt]/dt = k_1[^3D][cyt] - (k_{1b} + k_{et})[^3D{:}cyt] \quad (2a)$$

where the concentration of ^3D will evolve with time according to the differential equation

$$d[^3D]/dt = k_{1b}[^3D{:}cyt] - k_1[^3D][cyt] - k_3[^3D] \quad (2b)$$

To obtain the concentration of the bound DMNPAA:cytochrome *c* complex, the coupled differential equations in eq 2 must be solved, with the following initial conditions for ^3D, namely, $[^3D]_0$ is proportional to the initial concentration of the photoreductant, $[D]_0$, the laser power, as well as the duration of laser excitation of the sample. Substituting the result for $[^3D{:}cyt]$ back into eq 1 and integrating over time yield the following integrated rate expression for Scheme 2:

$$[cyt^-(t)] = \left[\frac{\Delta A_{550}k_{et}k_1{\cdot}cyt_0[^3D]_0}{[(k_{1b}+k_{et})(k_1{\cdot}cyt_0+k_3)-k_{1b}k_1{\cdot}cyt_0]{\cdot}2\Phi}\right]\times$$

$$[(\psi-\Phi)\exp(\{\psi+\Phi\}t)-(\psi+\Phi)\exp(\{\psi-\Phi\}t)+2\Phi) \quad (3)$$

where

$$\Phi = {}^1/_2\sqrt{(k_{1b}+k_{et})^2+2k_{1b}k_1{\cdot}cyt_0-2k_1{\cdot}cyt_0{\cdot}k_{et}-2k_3k_{1b}-2k_3k_{et}+(k_1{\cdot}cyt_0+k_3)^2}$$

$$\psi = -{}^1/_2(k_{1b}+k_{et}+k_1{\cdot}cyt_0+k_3)$$

and ΔA_{550} is the molar absorption coefficient for reduced minus oxidized cytochrome *c*.

In an attempt to determine the individual rate constants k_1, k_{1b}, k_3, and k_{et}, the observed electron transfer to cytochrome *c* was measured as a function of cytochrome *c* concentration from 3 to 60 μM. A global fitting for one exclusive set of rate constants to all eight experimentally obtained transient kinetic traces at different cytochrome *c* concentrations to the kinetic model described by eq 3 was attempted using a Levenberg-Marquardt least-squares fitting routine. However, no convergent global solution was obtained. This indicated that either the kinetic model proposed in Scheme 2 was incorrect (other processes unaccounted for in Scheme 2) or that the solution to the kinetic model (eq 3) was too complex to be solved (the fitting routine could not escape a local minima from the various initial guesses) for the limited cytochrome *c* concentrations attainable in these experiments. Because the photochemistry of the nitrobenzene derivatives is not fully understood at this time, it is quite possible that other processes exist which further complicate the kinetic model given in Scheme 2. We have, for example, neglected any effects of cytochrome *c* concentration on the quantum yield of production of the triplet donor. Additional processes such as a bimolecular and unimolecular quenching of the complexed intermediate have been added to the kinetic mechanism (Scheme 3) where k_{bm} and k_{um} represent

SCHEME 3

$$[^3D{:}cyt] + cyt \xrightarrow{k_{bm}} [D{:}cyt] + cyt$$

$$[^3D{:}cyt] \xrightarrow{k_{um}} [D{:}cyt]$$

the bimolecular and unimolecular rate constants, respectively. The new coupled set of differential equations which include these additional steps in the kinetic mechanism were solved as described above. The resulting kinetic expressions were again used in the global fitting of the eight experimental kinetic decay curves. However, no global fit was found when either one or both of these additional processes were included in the kinetic scheme. Introduction of further reaction pathways into the kinetic model seemed unwarranted given our current understanding of the nitrobenzene photochemistry.

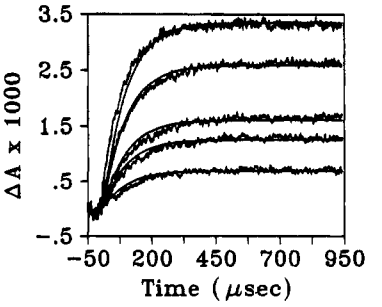

Figure 9. Concentration dependence of the transient absorption photoreduction of cytochrome *c* at 550 nm by DMNPAA. The five transient kinetic traces shown are for increasing concentrations of cytochrome *c*: 3 μM (lower trace), 6 μM, 7.5 μM, 15 μM, and 30 μM (upper trace). The transient kinetic traces for 45 and 60 μM cytochrome *c* are not shown for clarity since the transient signals are smaller than for 30 μM. The fit to each kinetic trace is from eq 3 using the parameters from the average rate constants given in Table 3. The experimental conditions were the same as in Figure 2 and the transients are an average of five laser shots.

TABLE 3: Average Least-Squares Fit to Eq 3 for the Cytochrome *c* Dependent Kinetic Traces

parameter	average fit	standard deviation
k_1	3.27×10^7 s^{-1} M^{-1}	2.05×10^6
k_{1b}	1.04×10^5 s^{-1}	4.23×10^3
k_3	1.11×10^4 s^{-1}	2.86×10^3
k_{et}	1.46×10^4 s^{-1}	1.44×10^3
$^3D_0$	3.63×10^{-5} M	4.39×10^{-6}

When each of the eight experimental kinetic decay curves at different cytochrome *c* concentrations were fit independently to eq 3, two consistent solutions were obtained. Each solution had similar rate constants for all eight experimentally measured kinetic traces. However, one set of rate constants was not evaluated further since k_1 was at the diffusion limit and did not seem feasible for the observed chemistry. The second set is given in Table 3. The fit and standard deviation listed in Table 3 for each rate constant is the average from all eight independent fits over the varied cytochrome *c* concentrations. Figure 9 shows the fit to the experimental kinetic decay curves using the average rate constants given in Table 3. The only factor in eq 3 which is not constant for all fits to the experimental kinetic curves is the amplitude of the photoexcited DMNPAA, $[^3D]_0$. Attempts were made to correct the yield of photoexcited DMNPAA because of the increased number of photons absorbed by the increasing cytochrome *c* concentration. However, models using the molar absorption coefficients for cytochrome *c* and DMNPAA at 355 nm were unsuccessful in correcting the discrepancy in the yield of $[^3D]_0$ found in the kinetic fitting routine. These results seem to indicate a competitive process between cytochrome *c* or some other quenching species for the photoexcited DMNPAA electron donor. This competitive side reaction has not been identified, although the most obvious candidate is quenching of the excited singlet state by cytochrome *c* via processes other than intersystem crossing. Another possibility is variable quenching of the excited state (singlet or triplet) by exogenous metals in solution as described previously. Despite the small discrepancy in the calculated excited DMNPAA concentration for the various concentrations of cytochrome

c, the kinetic model provides a satisfactory simulation of the cytochrome c photoreduction and the experimentally determined binding constants (K_D > 1000 μM), and we obtain a value of 1.46×10^4 s^{-1} for the unimolecular electron-transfer rate constant (k_{et}) when DMNPAA is employed as the photoreductant.

Unimolecular Limit of the Reaction Kinetics. The solution to the kinetic model (Scheme 2) results in two exponential terms for the bimolecular reaction (eq 3). However, when the rate constants determined from the simulation for DMNPAA (Table 3) are inserted into eq 3, the two exponential components are different in both their amplitude and decay rate. The first exponential, $[\exp(\Psi + \Phi)t]$, has roughly a 90% amplitude and ~100 μs time constant while the second exponential, $[\exp(\Psi - \Phi)t]$, has roughly a 10% amplitude and ~10 μs time constant. The sum of these two exponentials is essentially a single ~100 μs exponential decay except at very short times. Even then, the deviations are sufficiently small that they cannot be detected within experimental error. Therefore, under the experimental conditions used in this work, a single-exponential fit satisfactory approximates the kinetic model and corresponds to the fits listed in Table 1 for the observed rate constants.

Effect of Electrostatic Interactions on Electron Transfer. The one major drawback with these donors thus far is that the observed electron-transfer rate is relatively slow under the high ionic strength conditions used to study the electron input into cytochrome c ($k_{obs} \approx 10\,000$ s^{-1}). For hemoglobin, myoglobin, and peroxidase, the observed electron-transfer rate is even slower for the same experimental conditions and concentration of substrates (Table 2). One possible explanation for these observed rates is the electrostatic interaction between the DMNPAA donor and the protein acceptor. Under the pH conditions in which the electron-transfer rates were measured (pH 6.6), DMNPAA is deprotonated and has a negative charge from the carboxyl group. The isoelectric point (pI) for the four proteins studied here are: pI = 10.4 for cytochrome c, pI = 7.7 for myoglobin, pI = 6.8 for hemoglobin, and pI = 7.2 for peroxidase. This means that DMNPAA would have the greatest electrostatic interaction with cytochrome c, then myoglobin, peroxidase, and hemoglobin the weakest binding. The observed electron-transfer rates approximately follow this ordering except that hemoglobin and peroxidase are reversed in regard to their electron-transfer rates. If this trend turns out to be correct, then these donors can be easily modified synthetically to have more positive or negative charges as substituents to complement the charge on the protein of interest and increase the electrostatic interaction and ultimately the electron-transfer rates.

Another factor that affects the electron transfer from the nitrobenzene derivatives to the various proteins is the accessibility of the heme crevice to the electron donors. Even though the isoelectric point for *Paracoccus denitrificans* cytochrome 550 (pI = 3.5) is much lower than for horse cytochrome c (pI = 10.4), the observed electron-transfer rate from DMNPAA under identical concentrations is the same within experimental error (data not shown). This apparent discrepancy is easily explained by noting that the heme crevice for both horse cytochrome c and *Paracoccus denitrificans* cytochrome 550 is highly positively charged[34] due to the presence of several lysine residues in this region of the protein. Therefore, the charge in the heme crevice and the binding affinity for the photoreductant is the same for both cytochromes even though the overall isoelectric point of the two proteins varies substantially. The positively charged domain surrounding the heme is therefore the major contributor influencing the intermolecular electron transfer because it dominates the electrostatic interaction between the donor and acceptor.

Although the data (Table 1) do not show an exact correlation between the observed electron-transfer rate and charge on the donor, the trend is certainly clear. The negatively charged donors exhibit the fastest observed rates, and the neutral and the positively charged donors are slower. This correlation is remarkably good considering that the charged group is not the only substituent varying among the various donors examined, and the other substituents may also have some effect on the electron-transfer and binding processes. Through the manipulation of the side chains and charged groups on these electron donors, these nitrobenzene derivatives could be used to make "designer" electron donors to a wide variety of proteins.

pH and Ionic Strength Dependence on Electron Transfer. The pH dependence and the ionic strength dependence results can be rationalized in terms of the same electrostatic model mentioned above. As the pH increases, the electron donor is essentially unaffected since the pK_a of the acid is lower than the lowest pH used in these experiments. However, the increasing pH causes the effective positive charge on cytochrome c to decrease, thus decreasing the electrostatic interaction between the donor and protein and causing the observed electron-transfer rate to decrease with increasing pH. Following similar reasoning, when the ionic strength decreases, there is enhanced binding between the electron donor and the protein. In the limit of a bound donor:protein complex, the electron-transfer rate would approach its fastest possible rate. Under these conditions, the process becomes unimolecular with $k_{obs} = k_{et}$, and the kinetics are not limited by the collision rate. Under high ionic strengths, the reaction should be second order with a slower observed electron-transfer rate.

The data for the ionic strength dependence are consistent with the above model. DMNPAA has a single acid functionality and does not form a tight complex with cytochrome c (K_D > 1000 μM at 5 mM ADA) and would be expected to have little ionic strength dependence in agreement with the small changes observed in the experimental data. The triacid DANPATA, on the other hand, has three negative carboxyl groups which should bind much tighter to the positively charged cytochrome c ($K_D = 70 \pm 5$ μM at 5 mM ADA). Accordingly, as the ionic strength decreases, the observed electron-transfer rate increases significantly from $k_{obs} = 6100$ s^{-1} at 200 mM ADA to $k_{obs} = 36\,000$ s^{-1} at 20 mM ADA (Figure 7). In addition to the large increase in the observed rate with decreasing ionic strength, a smaller overall ΔA signal is observed. This could be interpreted as the DANPATA donor having several tight binding sites on cytochrome c with only one which is an electron-transfer-competent site. So even though the number of DANPATA donors which are tightly bound increases, the protein is capable of accepting only one electron, thus the overall ΔA observed decreases. The remaining bound photoexcited donors presumably become deactivated via radiative or rearrangement processes. It should be noted, however, that those donors which are in the electron-transfer-competent site should exhibit a dramatically increased observed electron-transfer rate, probably approaching the unimolecular electron-transfer rate constant k_{et}. Another possible explanation for the decreased yield is the effect of the ADA buffer on the electron-transfer yield as mentioned before. The yield of reduced cytochrome c is consistently greater in ADA buffer than in phosphate, HEPES, or Tris·HCl, although equivalent yields have been observed on occasion for these alternative buffers. Thus the decrease in the yield of reduced cytochrome c may be due to the decrease in yield caused by the lower ADA concentration used for the ionic strength dependence and not from multiple tight-binding sites.

Even with this caveat, the results confirming the increased electron-transfer rates as the donor:acceptor complex becomes more tightly bound remains true.

General Utility for Studying Enzymatic Reactions. The principal motivation for this work was to develop a photoreductant which would enable us to study the electron transfer between cytochrome *c* and cytochrome *c* oxidase during the turnover of dioxygen to water under physiological conditions. Recent work by Millett and co-workers[29] and Nilsson[35] have found that the electron input from cytochrome *c* to Cu_A in cytochrome *c* oxidase is greater than 10^5 s^{-1}. This electron input rate is faster than the observed photoreduction of cytochrome *c* by these new nitrobenzene photoreductants reported in this work and suggest that the nitrobenzene photoreductants could not be used to study this enzymatic reaction. However, this is not the case. The experiments by Millett and co-workers[29] and Nilsson[35] were studied under low ionic strengths where cytochrome *c* and cytochrome *c* oxidase form a tight 1:1 electrostatic complex. The electron-transfer mechanism may be different and slower for the physiological process, as shown by the much slower input rates into heme *a* under physiological ionic strengths.[24,36,37]

Even if the electron input rate was greater than 10^5 s^{-1} under physiological conditions, the nitrobenzene photoreductants could be modified to increase the electron-transfer rate to cytochrome *c*. One method would be to put on more negative charges to increase the electrostatic complexation between the nitrobenzene photoreductant and cytochrome *c* at physiological ionic strength. Our results reported here have shown that the electrostatic binding between the nitrobenzene photoreductant and cytochrome *c* increases as more negative charges are placed on the nitrobenzene framework (DANPATA triacid) and the observed electron-transfer rate increases to 36 000 s^{-1} when the tighter complex forms. Increasing the number of negative charges on the photoreductant would increase the binding constant and ultimately increase the electron-transfer rate constant, where the limiting rate would be determined by the inherent intramolecular electron-transfer rate constant, k_{et}.

A second method would be to covalently link the nitrobenzene photoreductant to cytochrome *c* by well-known coupling reactions to form an intramolecular photoreductant similar to the Ru–cytochrome *c* derivatives used by Millett and co-workers.[29] Then the limiting effect for the photoreduction of cytochrome *c* would not be the bimolecular collision rate as observed for this work at high ionic strength. The unimolecular electron transfer could be substantially greater than the bimolecular rate for the electron transfer from cytochrome *c* to cytochrome *c* oxidase at physiological ionic strength (no tight 1:1 electrostatic complex is formed). Then the electron-transfer rate between these new nitrobenzene photoreductants and cytochrome *c* would not be limiting in studying the physiological electron transfer between cytochrome *c* and cytochrome *c* oxidase. These photoreductants could also be used with other enzymatic systems using a similar methodology.

Conclusions

Substituted nitrobenzene derivatives, which were previously used as protecting groups in organic chemistry and for the photoinitiated release of substrates, have been successfully adapted as effective photoreductants for proteins as shown with cytochrome *c* and other heme proteins. In addition, they can be synthetically modified to function as photoreductants for other proteins as well. We have shown that the photoreductant can be engineered by increasing the number of negatively charged substituents on the nitrobenzene framework (DMNPAA to DANPATA) to increase the electrostatic interaction and increase the observed electron-transfer rate from ~9000 s^{-1} to 36 000 s^{-1} for the photoreduction of cytochrome *c*. The general utility of these nitrobenzene photoreductants is being extended by using them to initiate intermolecular electron transfer between two physiological redox proteins.

Experimental Section

Transient Absorption Spectroscopy. Stock solutions of the photoreductants were 10 mM in H_2O/methanol and stored at −80 °C until needed. Typical transient absorption samples contained 980 μL of 100 mM ADA buffer at pH 6.6, 10 μL of 10 mM photoreductant (100 μM), and 10 μL of 1.5 mM cytochrome *c* (15 μM) in a 1 cm quartz cuvette with a micro stir bar. Cytochrome *c* was photoreduced by exciting the photoreductant at 355 nm with the third harmonic from a Spectra Physics DCR-12 Nd:YAG laser. The excitation pulse typically had a 10–20 ns pulse width (fwhm) and an output power of 1.5 mJ/pulse at the sample. The Nd:YAG flash lamp was fired at a 10 Hz repetition rate but the Q-switch was externally triggered at 1 Hz to achieve a 1 Hz laser pulse repetition rate. The probe source for the transient absorption spectra was a 75 W xenon arc lamp which passed through a 530 nm Schott glass long-pass filter before the sample and the transmitted light was passed through a second 530 nm Schott glass long-pass filter before going through an Instruments SA 1690B double monochromator set at 550 nm and detected with a photomultiplier tube. The transient signal was amplified with a Keithly 427 current amplifier and digitized using a Tektronix R710 200 MHz transient digitizer interfaced to a microcomputer.

Materials. Horse heart cytochrome *c* (Sigma), horse heart myoglobin (Sigma), horseradish peroxidase (Sigma), human hemoglobin (Sigma), and *N*-2-acetamidoiminodiacetic acid (ADA, Calbiochem) were used without further purification.The photoreductants 2-nitrophenylacetic acid (NPAA), 4,5-dimethoxy-2-nitrobenzaldehdye (DMNB), 4,5-dimethoxy-2-nitrobenzoic acid (DMNBA), and 5,5′-dithiobis(2-nitrobenzoic acid) (DTBNBA) were purchased from Aldrich and used without further purification. γ-Aminobutyric acid, 4,5-dimethoxy-2-nitrobenzyl ester, hydrochloride (GABA) was purchased from Molecular Probes and used without further purification.

Synthesis. Tetrahydrofuran was refluxed over sodium metal/benzophenone and freshly distilled prior to use. All other solvents were of reagent grade or better and used without further purification. Proton NMR data were collected on a Bruker AM 500 or a GE QE 300 using a deuterium lock. IR spectra were taken on a Perkin-Elmer 1600 FTIR. GCMS was performed on a Hewlett-Packard 5890A gas chromatograph equipped with a 12 m silicon gum capillary column coupled to a 5970 Series mass-sensitive detector. Absorption spectroscopy was performed on a Hewlett-Packard 8452A diode array spectrophotometer.

4,5-Dimethoxy-2-nitrophenylacetic Aspartamide (DMNPA-ASP, 1). 4,5-Dimethoxy-2-nitrophenylacetic acid (0.18 g, 0.77 mmol) was dissolved in 5 mL of CH_2Cl_2 and 3 mL of DMF and cooled to 0 °C in an ice bath. Dicyclocarbodiimide (0.16 g, 0.77 mmol) was added dropwise and stirred for 90 min. Aspartic acid (0.12 g, 0.94 mmol) in 1 mL of DMF was added to this solution at 0 °C, then the reaction mixture was allowed to warm to room temperature and stirred for 24 h. The resultant precipitate was filtered, the filtrate was quenched with 20 mL of H_2O, extracted with ethyl acetate (3 × 40 mL), and dried with $MgSO_4$, and solvent was removed in vacuo. The resultant solid was recrystallized from ethyl acetate to yield a light yellow powder. Absorption spectrum (water) λ_{max} ($\epsilon_M \times 10^{-3}$ M^{-1} cm^{-1}) 349 nm (6.3); ^1H NMR (acetone-d_6, 300 MHz) δ 7.65 (s, 1 H), 6.97 (s, 1 H), 4.13 (s, 2 H), 3.88 (s, 6 H), 2.79 (m, 1 H), 1.76 (m, 1 H), 1.31 (m, 1 H).

1-(4,5-Dimethoxy-2-nitrophenyl)ethyl-1-succinic Acid (SUCC, 2). Succinic acid (0.944 g, 8.0 mmol) was added to 20 mL of DMF, and the resultant heterogeneous mixture was stirred at room temperature. 1-(4,5-Dimethoxy-2-nitrophenyl)-1-diazaethane (25 mg, 0.2 mmol, prepared according to the procedure described by Molecular Probes) dissolved in chloroform was added dropwise to the heterogeneous solution. The dark orange color of the diaza solution slowly faded during the addition, and the solution was stirred for 4 h at room temperature. The resulting pale yellow solution was lyophilized, and the resulting solid was dissolved in 25 mL of 5:1 $CHCl_3$:THF and washed with water (4 × 10 mL). The organic layer was collected, and the solvent removed in vacuo to yield a yellow oil. This oil was purified by preparative TLC using 10:1 $CHCl_3$:THF (R_f 0.4). The product was extracted from the silica with THF, and the solvent removed in vacuo. Concentrated NH_4OH (3 drops), water (5 mL), and $CHCl_3$ (5 mL) were added to the product. The aqueous layer was washed with $CHCl_3$ (2 × 5 mL) and lyophilized to yield 0.0212 g of a pale yellow powder. Absorption spectrum (water) λ_{max} ($\epsilon_M \times 10^{-3}$ M^{-1} cm^{-1}) 347 nm (5.7), 310 nm (sh); ^1H NMR (methanol-d_4, 300 MHz) δ 7.57 (s, 1 H), 7.15 (s, 1 H), 6.34 (q, 1 H, J = 6.3 Hz), 3.97 (s, 3 H), 3.87 (s, 3 H), 2.60 (m, 2 H), 2.47 (m, 2 H), 1.59 (d, 3 H, J = 6.3 Hz).

Methyl-4,5-dimethoxy-2-nitrophenylacetate (MDMNPA, 3). 4,5-Dimethoxy-2-nitrophenylacetic acid (2.67 g, 11.1 mmol) was suspended in 150 mL of methanol. $SOCl_2$ (1.5 mL, 20.6 mmol) was added dropwise and stirred overnight at room temperature. The precipitated ester was vacuum filtered and washed with cold methanol to yield 1.68 g of a light yellow powder (60%); mp 108−109 °C; IR 1723.1 cm^{-1}; MS calculated for $C_{11}H_{13}NO_6$ 210, *m/e* found 210; absorption spectrum (water) λ_{max} ($\epsilon_M \times 10^{-3}$ M^{-1} cm^{-1}) 348 nm (6.6), 310 nm (sh); ^1H NMR ($CDCl_3$, TMS, 500 MHz) δ 7.79 (s, 1 H), 6.79 (s, 1 H), 4.05 (s, 2 H), 4.00 (s, 3 H), 3.98 (s, 3 H), 3.75 (s, 3 H).

4,5-Dimethoxy-2-nitroacetophenone (DMNAP, 7). 3,4-dimethoxyacetopheneone (14.98 g, 83.2 mmol) was added over 1 h to 90 mL of concentrated HNO_3 and stirred for an additional 1 h, maintaining the temperature between 18 and 22 °C. The solution was poured into 1200 mL of H_2O and chilled in an ice bath. The precipitated crystals were collected by vacuum filtration and recrystallized from H_2O and then ethanol to yield 10.97 g (59%) of yellow needles; mp 131−132 °C; MS calculated for $C_{11}H_{13}NO_5$ 239, *m/e* found 239; absorption spectrum (water) λ_{max} ($\epsilon_M \times 10^{-3}$ M^{-1} cm^{-1}) 349 nm (5.6), 309 nm (sh); ^1H NMR ($CDCl_3$, TMS, 500 MHz) δ 7.61 (s, 1 H), 6.78 (s, 1 H), 3.99 (s, 6 H), 2.50 (s, 3 H).

4,5-Dimethoxy-2-nitrophenylacetic Acid (DMNPAA, 8). 3,4-Dimethoxy-2-phenylacetic acid (5.12 g, 26.1 mmol) was dissolved in 50 mL of glacial acetic acid at 0 °C in an ice bath. Concentrated HNO_3 (67%, 30 mL) was added dropwise with stirring and then allowed to react for 2 h at 0 °C. The solution was poured into 1 L of saturated NaCl solution, and the product immediately precipitated from solution and was vacuum filtered and washed with cold H_2O to yield 5.34 g of yellow powder (85%). MS calculated for $C_{10}H_{11}NO_6$, *m/e* 241, found 241; absorption spectrum (water): λ_{max} ($\epsilon_M \times 10^{-3}$ M^{-1} cm^{-1}) 350 nm (5.4), 310 nm (sh); ^1H NMR (acetone-d_6, 300 MHz) δ 10.89 (s, 1 H), 7.75 (s, 1 H), 7.15 (s, 1 H), 4.08 (s, 2 H), 3.99 (s, 3 H), 3.97 (s, 3 H).

4,5-Dimethylalkyl-2-phenylalkyl Acetate (DMAPA, 9a). 3,4-Dihydroxyphenylacetic acid (2.19 g, 12.03 mmol) was dissolved in 75 mL of DMF. K_2CO_3 (4.99 g, 36.08 mmol) was added to the solution, then 3.42 mL (36.08 mmol) of bromo acetate (Aldrich) was added dropwise, and the reaction mixture stirred at room temperature for 24 h. The reaction was quenched with 100 mL of H_2O and extracted with ethyl acetate (3 × 100 mL). The combined organic layers were dried with $MgSO_4$, and solvent was removed in vacuo at room temperature. The product was purified by flash silica chromatography (diethyl ether) to yield 2.96 g (61%) of clear oil. MS calculated for $C_{17}H_{20}O_{10}$ 384, *m/e* found 384; ^1H NMR ($CDCl_3$, 300 MHz) δ 6.78 (m, 3 H), 4.63 (s, 2 H), 4.61 (s, 2 H), 4.52 (s, 2 H), 3.68 (s, 3 H), 3.67 (s, 3 H), 3.63 (s, 3 H), 3.55 (s, 2 H).

4,5-Dimethylalkyl-2-nitrophenylalkyl Acetate (DMANPA, 9b). 4,5-Dimethylalkyl-2-phenylalkyl acetate (0.38 g, 1.0 mmol) was dissolved in 15 mL of glacial acetic acid and 8 mL of concentrated HNO_3 was added dropwise with stirring at room temperature. After 8 h, 50 mL of H_2O was added, and the reaction mixture extracted with diethyl ether (3 × 30 mL). The combined organic layers were dried with $MgSO_4$, and solvent was removed in vacuo at room temperature. The product was purified by flash silica chromatography (diethyl ether) to yield 0.33 g (79%) of the light yellow oil. MS calculated for $C_{17}H_{19}NO_{12}$, *m/e* 429, found 429; ^1H NMR (acetone-d_6, 300 MHz) δ 7.72 (s, 1 H), 6.80 (s, 1 H), 4.84 (s, 2 H), 4.79 (s, 2 H), 4.66 (s, 2 H), 4.08 (s, 2 H), 3.82 (s, 3 H), 3.81 (s, 3 H), 3.76 (s, 3 H).

4,5-Dialkyl-2-nitrophenylacetic Triacid (DANPATA, 9). 4,5-Dimethylalkyl-2-phenylalkyl acetate (1.17 g, 3.0 mmol) was dissolved in 15 mL of glacial acetic acid and 15 mL of concentrated HNO_3 was added dropwise at room temperature with stirring. After 48 h, 50 mL of H_2O was added and the reaction mixture extracted with ethyl acetate (3 × 75 mL). The combined organic layers were dried with $MgSO_4$, and solvent was removed in vacuo at room temperature. The product was recrystallized twice from ethyl acetate to yield 0.65 g of light yellow powder (55%). Absorption spectrum (water): λ_{max} ($\epsilon_M \times 10^{-3}$ M^{-1} cm^{-1}) 346 nm (5.7), 308 nm (sh); ^1H NMR (acetone-d_6, 300 MHz) δ 7.80 (s, 1 H), 7.21 (s, 1 H), 4.96 (s, 2 H), 4.94 (s, 2 H), 4.65 (s, 2 H), 4.13 (s, 2 H).

4,5-Dimethylalkyl-2-nitrophenylacetic Acid (DMANPAA, 10). NaOH (1 N, 5 mL) was added to 4,5-dimethylalkyl-2-nitrophenylalkyl acetate (0.30 g, 0.7 mmol) and stirred for 8 h at room temperature. H_2O (10 mL) was added, and the reaction mixture extracted with ethyl acetate (3 × 25 mL). The combined organic layers were dried with $MgSO_4$, and solvent was removed in vacuo at room temperature. The product was purified by flash silica chromatography (2:3, hexanes:acetone) to yield a white powder. Absorption spectrum (water): λ_{max} ($\epsilon_M \times 10^{-3}$ M^{-1} cm^{-1}) 335 nm (3.8), 298 nm (sh); ^1H NMR (acetone-d_6, 300 MHz) δ 7.61 (s, 1 H), 6.80 (s, 1 H), 4.81 (s, 2 H), 4.77 (s, 2 H), 4.12 (s, 2 H), 3.87 (s, 6 H).

4,5-Dihydroxy-2-nitrophenylacetic Acid (DHNPAA, 12) and 3,4-Dihydroxy-1,6-dinitrophenylacetic Acid (DHDNPAA, 13). H_2O (15 mL) was added to 3,4-dihydroxyphenylacetic acid (0.50 g, 2.97 mmol) and sodium nitrite (0.68 g, 9.92 mmol) and stirred at room temperature. Concentrated H_2SO_4 (1 mL) was added dropwise and stirred for 1 h and then reaction extracted with ethyl acetate (3 × 75 mL). The combined organic layers were dried over $MgSO_4$, and solvent was removed in vacuo. The products were purified by flash silica chromatography (1:1 ethyl acetate:diethyl ether) to yield 0.26 g (41%) 4,5-dihydroxy-2-nitrophenylacetic acid (R_f 0.6; absorption spectrum (water) λ_{max} ($\epsilon_M \times 10^{-3}$ M^{-1} cm^{-1}) 383 nm (4.4); ^1H NMR (acetone-d_6, 300 MHz) δ 7.64 (s, 1 H), 6.86 (s, 1 H), 3.87 (s, 2 H)) and 0.22 g (29%) of 3,4-dihydroxy-1,6-dinitrophenylacetic acid (R_f 0.2; absorption spectrum (water) λ_{max} ($\epsilon_M \times 10^{-3}$ M^{-1} cm^{-1}) 427 nm (5.6); ^1H NMR (acetone-d_6, 300 MHz) δ 7.09 (s, 1 H), 3.85 (s, 2 H)).

Acknowledgment. We would like to thank Dr. Jay Winkler for his assistance with the nanosecond transient absorption apparatus in the Beckman Institute Laser Resource Center. This

work was supported by grant GM22432 from the National Institute of General Medical Sciences, U. S. Public Health Service. TJD is the recipient of a National Research Service Award from the National Institute of General Medical Sciences (GM15647).

References and Notes

(1) Somlyo, A. P.; Somlyo, A. V. *Annu. Rev. Physiol.* **1992**, *52*, 857–874.
(2) Homsher, E.; Millar, N. C. *Annu. Rev. Physiol.* **1992**, *52*, 875–896.
(3) Thirlwell, H.; Corrie, J. E. T.; Reid, G. P.; Trentham, D. R.; Ferenczi, M. A. *Biophys. J.* **1994**, *67*, 2436–2447.
(4) Kaplan, J. H.; Forbush, B. III; Hoffman, J. F. *Biochemistry* **1978**, *17*, 1929–1935.
(5) Buchet, R.; Jona, I.; Martonasi, A. *Biochim. Biophys. Acta* **1992**, *1104*, 207–214.
(6) Tanner, J. W.; Thomas, D. D.; Goldman, Y. E. *J. Mol. Biol.* **1992**, *223*, 185–203.
(7) Kozlowski, R. Z.; Twist, V. W.; Brown, A. M.; Powell, T. *Am. J. Physiol.* **1991**, *261*, H1665–H1670.
(8) Dolphin, A. C.; Wootton, J. F.; Scott, R. H.; Trentham, D. R. *Pflügers Arch.* **1988**, *411*, 628–636.
(9) Ellisdavies, G. C. R.; Kaplan, J. H. *Proc. Natl. Acad. Sci. U.S.A.* **1994**, *91*, 187–191.
(10) Adams, S. R.; Kao, J. P. Y.; Tsien, R. Y. *J. Am. Chem. Soc.* **1989**, *111*, 7957–7968.
(11) Corrie, J. E. T.; Trentham, D. R. *Bioorganic Photochemistry*; Morrison, H., Ed.; Wiley Press: New York, 1993, Vol. 2, pp 243–305.
(12) Hess, B. P. *Biochemistry* **1993**, *32*, 989–1000.
(13) Wieboldt, R.; Ramesh, D.; Carpenter, B. K.; Hess, B. P. *Biochemistry* **1994**, *33*, 1526–1533.
(14) Wieboldt, R.; Gee, K.; Niu, L.; Ramesh, D.; Carpenter, B. K.; Hess, B. P. *Proc. Natl. Acad. Sci. U.S.A.* **1994**, *91*, 8752–8756.
(15) Snyder, R.; Trotter, W.; Testa, A. C. *J. Lumin.* **1985**, *33*, 327–332.
(16) Kobayashi, K.; Hayashi, K. *Fast Methods in Physical Biochemistry and Cell Biology*; Sha'afi, R., Fernandez, R., Eds.; Elsevier North-Holland Biomedical Press: Amsterdam, 1983, pp 87–111.
(17) Van Buuren, K. J. H.; Van Gelder, B. F.; Wilting, J.; Braams, R. *Biochim. Biophys. Acta* **1974**, *333*, 421–429.
(18) Pecht, I.; Faraggi, M. *Nature* **1971**, *233*, 116–118.
(19) O'Neil, P.; Fielden, E. M.; Finazzi-Argo, A.; Aviglicino, L. *Biochem. J.* **1983**, *209*, 167–174.
(20) Anderson, R. F.; Hille, R.; Massey, V. *J. Biol. Chem.* **1986**, *261*, 15870–15876.
(21) Kobayashi, K.; Une, H.; Hayashi, K. *J. Biol. Chem.* **1989**, *264*, 7976–7980.
(22) Cho, K. C.; Che, C. M.; Ng, K. M.; Choy, C. L. *J. Am. Chem. Soc.* **1986**, *108*, 2814–2818.
(23) Zhou, J. S.; Granada, E. S. V.; Leontis, N. B.; Rodgers, M. A. J. *J. Am. Chem. Soc.* **1990**, *112*, 5074–5080.
(24) Hazzard, J. T.; Rong, S.-Y.; Tollin, G. *Biochemistry* **1991**, *30*, 213–221.
(25) Tollin, G.; Hurley, J. K.; Hazzard, J. T.; Meyer, T. E. *Biophys. Chem.* **1993**, *48*, 259–279.
(26) Brunschwig, B. S.; Delaive, P. J.; English, A. M.; Goldberg, M.; Mayo, S. L.; Sutin, N.; Gray, H. B. *Inorg. Chem.* **1985**, *24*, 3743–3749.
(27) Wishart, J. F.; Vaneldik, R.; Sun, J.; Su, C.; Isied, S. S. *Inorg. Chem.* **1992**, *31*, 3986–3989.
(28) Orii, Y. *Biochemistry* **1993**, *32*, 11910–11914.
(29) Pan, L. P.; Hibdon, S.; Liu, R.-Q.; Durham, B.; Millett, F. *Biochemistry* **1993**, *32*, 8492–8498.
(30) Wuttke, D. S.; Bjerrum, M. J.; Chang, I. J.; Winkler, J. R.; Gray, H. B. *Biochim. Biophys. Acta* **1992**, *1101*, 168–170.
(31) Czarnik, A. W. *Acc. Chem. Res.* **1994**, *27*, 302–308.
(32) Gu, Y. G.; Li, P. S.; Sage, J. T.; Champion, P. M. *J. Am. Chem. Soc.* **1993**, *115*, 4993–5004.
(33) Walker, J W.; Reid, G. P.; McCray, J. A.; Trentham, D. R. *J. Am. Chem. Soc.* **1988**, *110*, 7170–7177.
(34) Timkovich, R.; Dickerson, R. E. *J. Biol. Chem.* **1976**, *251*, 4033–4046.
(35) Nilsson, T. *Proc. Natl. Acad. Sci. U.S.A.* **1992**, *89*, 6497–6501.
(36) Larson, R. W.; Winkler, J. R.; Chan, S. I. *J. Phys. Chem.* **1992**, *96*, 8023–8027.
(37) Pan, L.-P.; Hazzard, J. T.; Lin, J.; Tollin, G.; Chan, S. I. *J. Am. Chem. Soc.* **1991**, *113*, 5908–5910.

JP9516304